Materials Letters 141 (2015) 100–103

Contents lists available at ScienceDirect

Materials Letters

journal homepage: www.elsevier.com/locate/matlet

Deposition of porous nano-WO_3 coatings with tunable grain shapes by liquid plasma spraying for gas-sensing applications

Qingfei Wu, Jing Huang, Hua Li *

Key Laboratory of Marine Materials and Related Technologies, Zhejiang Key Laboratory of Marine Materials and Protective Technologies, Ningbo Institute of Materials Technology and Engineering, Chinese Academy of Sciences, Ningbo 315201, China

ARTICLE INFO

Article history:
Received 23 August 2014
Accepted 15 November 2014
Available online 26 November 2014

Keywords:
Thick films
Deposition
Microstructure
WO_3
Liquid plasma spraying
Planar grain

ABSTRACT

Porous nanostructured WO_3 coatings were deposited by two routes, solution and suspension plasma spraying. The nanostructural characteristics of the coatings were tunable by adjusting the constituents of the starting liquid precursor and spray parameters. Planar or spherical WO_3 grains with controllable sizes in nano-scale have been fabricated. Complete formation of spherical WO_3 grains was attained during solution plasma spraying. Enhanced heating of the nano-WO_3 particles by augmenting plasma power gave rise to oriented WO_3 grain growth along (0 0 2) plane. The planar WO_3 grains with the dimension of ~50 nm, ~80 nm, and ~700 nm in thickness, width, and length respectively were fabricated by the suspension plasma spraying. The results provide clear insight into potential gas-sensing applications of the porous WO_3 coatings.

1. Introduction

In recent years, emissions of toxic gas such as NOx, CO, etcetera in many countries have been deteriorating. There are therefore urgent demands for developing economic portable sensing devices. Among the gas sensors, metal oxide semiconductor sensors attracted the most attentions owing to their advantages of promising environmental stability and high sensitivity and selectivity [1]. Previous studies have shown that WO_3 is an ideal NO_2 sensing material [2,3]. Many methods such as sol-gel [4], magnetron sputtering [5], pyrolysis [6], thermal evaporation [3], hydrothermal [7], chemical vapor deposition [8], and plasma spray [9] have been attempted for depositing WO_3 film, among which atmospheric plasma spray (APS) is competitive for cost-effective mass production and accurate control of microstructure of the coatings [10]. It was established that the structure of the coatings in nano-scale is desirable for high sensitivity of the sensors [7,11]. Searching appropriate techniques for fabricating the nanostructured coatings is one of the current research goals. In this letter, we proposed two technical routes, liquid precursor plasma spraying (LPPS) and suspension plasma spraying (SPS), for depositing nanostructured WO_3 coatings with tunable grain features of WO_3. And the microstructure of the coatings was elucidated.

2. Experimental

Tungsten chloride (WCl_6) (Aladdin Reagent Corporation, China) was used for pyrolysis synthesis of tungsten trioxide (WO_3) during plasma spraying. The synthesis route has been evidenced effective in making WO_3 [12]. The WO_3 powder (Beijing DK Nano Technology Co. Ltd, China) with the particle size of ~40 nm was employed as the starting material for the SPS. For the LPPS, based on our previous systematic attempts on the use of several solvents, polyethylene glycol (PEG) was chosen as the solvent to be dissolved in deionized water. WCl_6 was dissolved in anhydrous ethyl alcohol. After ultrasonic cleaning for 20 min, the dissolved WCl_6 was mixed with the PEG solution under constant magnetic stirring. The pH value of the mixture was stabilized at ~7 as adjusted by ammonia hydroxide solution. For the WO_3 suspension preparation, WO_3 particles were dispersed in the mixture of anhydrous ethanol and water with certain amount of PEG. No dispersant was used. The APS-2000K plasma spray system (Beijing Aeronautical Manufacturing Technology Research Institute, China) was employed for the coating deposition on silicon wafer of 20 mm × 10 mm in length and width respectively. Silicon wafer was extensively employed as the substrate to take advantage of silicon microsystems technology for developing small-size micromachined gas sensors [13].

Microstructure of the powder and coatings was characterized by field emission scanning electron microscopy (FESEM, Hitachi S-550N, Japan) and transmission electron microscopy (TEM, FEI Tecnai F20, the Netherlands). Phase constitutions were detected by X-ray diffraction (XRD, PANalytical X'pert Pro MPD diffractometer, the Netherlands) at a

* Corresponding author. Tel.: +86 574 86686224; fax: +86 574 86685159.
E-mail address: lihua@nimte.ac.cn (H. Li).

http://dx.doi.org/10.1016/j.matlet.2014.11.072
0167-577X/

scan rate of 0.02°/s over a 2θ range of 10°–80° using Cu Kα radiation operated at 35 mA and 40 kV. Fourier transform infrared spectroscopy (FTIR, Nicolet 6700, Thermo Fisher Scientific, USA), Raman spectrometry (Renishaw inVia Reflex, Britain) and X-ray photoelectron spectroscopy (XPS, AXIS UTLTRADLD, Shimadzu, Japan) detection was also conducted for characterizing the samples. The infrared spectrum with a resolution of 4 cm and the scan number of 8 were adopted with a spectral region from 400 to 4000 cm^{-1}.

3. Results and discussion

The starting spherical WO_3 particles have the size of ~40 nm in diameter (Fig. 1a). Surprisingly, even though the use of the suspension as the starting feedstock alleviates the heating of the particles during the spraying, the particles still exhibit remarkable changes in shapes (Fig. 1). Interconnected grains with submicron-sized pores in between are clearly seen for all the coatings, which might benefit gas sensing performances [8,10]. The LPPS coatings show the nanostructures accumulated by spherical nanosized grains with the size of ~70 nm (Fig. 1b). Our extensive efforts have thus been devoted to investigating the effect of key spray parameters on the morphology of the grains. It was revealed that the power level plays the predominate role and ~33 kW power is a threshold value for accomplishing the planar shaped grains. The spraying with the power less than 33 kW resulted in the coatings comprising angular WO_3 grains (Fig. 1c). The contours of the grains changed from angular to planar with the dimension of ~70 nm and ~700 nm in thickness and width/length, respectively (Fig. 1d vs. c). Yet it is noted that there is almost no growth in thickness for the grains regardless of the changes of the spray power. Only significant growth along the directions of length and width of the grains was revealed. Moreover, for the coatings deposited with the power level of 30 kW, the grains essentially show a parallel-to-substrate state (Fig. 1c), while increased spray power resulted in the re-arrangement of the grains with the direction perpendicular to the substrate (Fig. 1d). This phenomenon might suggest that WO_3 grain growth took place along the direction perpendicular to the substrate surface. The oriented grain growth is similar to the columnar structure of thermal sprayed splats with internal grains being perpendicular to the substrate [14], which is likely attributed to the oriented cooling of the particles after their impingement on the substrate/pre-coating. In this study, the higher spray power level leads to enhanced heating of the particles, in turn giving rise to the bigger planar WO_3 grains. To further understand the oriented grain growth, the microstructure of the coatings has also been examined by high resolution TEM (Fig. 1e, f). The lattice fringe spacing of the grain at its largest surface is 0.39 nm, which is the lattice constant of the (0 0 2) plane of monoclinic WO_3. The TEM observation suggests that the growth of WO3 grains occurred during the coating deposition is along their (0 0 2) planes, which is the largest face in this case. Further XRD detection has confirmed the oriented growth of the WO_3 grains along their (0 0 2) plane (Fig. 2), which is further elucidated below.

XRD detection reveals the predominate presence of monoclinic WO_3 in the coatings (Fig. 2a). The augmented plasma power from 30 kW to 33 kW resulted in the oriented growth of the WO_3 grain along their (0 0 2) plane. The oriented growth was also recognized by other researchers [15]. This should account mainly for the altered contours of the grains as observed by EM characterization (Fig. 1). In addition, the LPPS coating consists of complete crystalline WO_3 (Fig. 2a). To clarify the stage at which WO_3 forms during the spraying, the starting precursor suspension was dried at 80 °C for 10 h for following XRD detection. The dried powder shows the presence of NH_4Cl, while no trace of WO_3 is seen (Fig. 2a), indicating clearly that monoclinic WO_3 was synthesized during the spraying. The reactions taking place during the plasma spraying are shown below [12]:

$$WCl_6 + C_2H_5OH \rightarrow W(C_2H_5O)_nCl_{6-n} + HCl \quad (1)$$

$$W(C_2H_5O)_nCl_{6-n} + H_2O \rightarrow WO_3 + C_2H_5OH + HCl \quad (2)$$

Further characterization by Raman spectroscopy confirms the sole component of WO_3 for all the coatings (Fig. 2b). The major

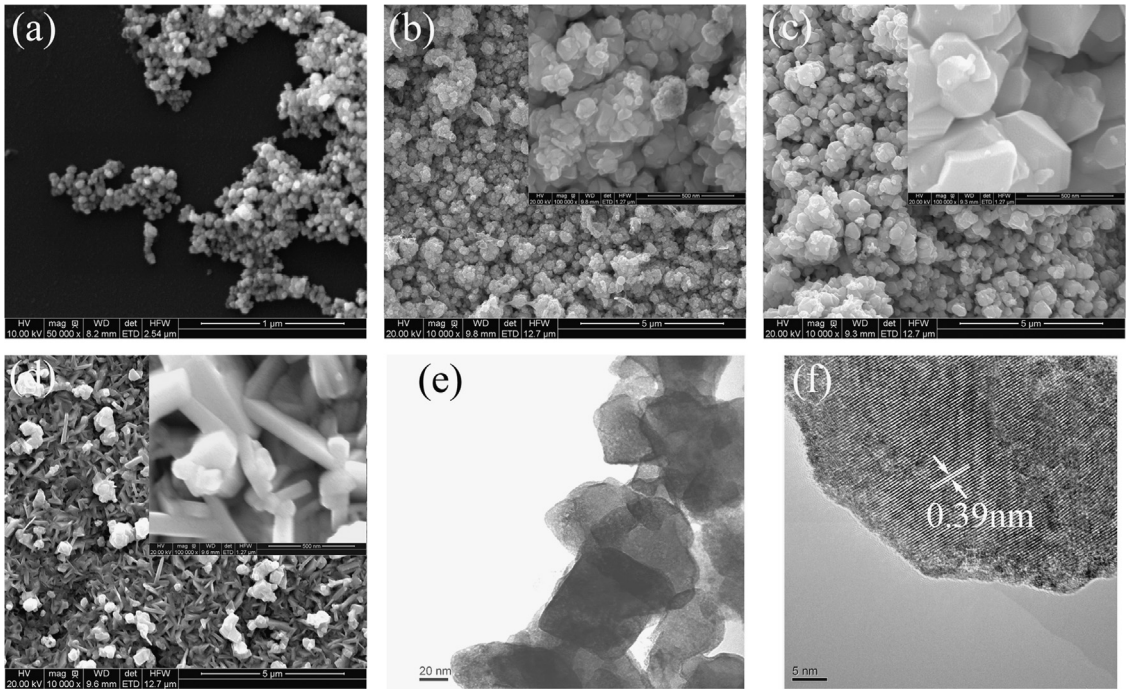

Fig. 1. Morphology of the powder and the coatings. FESEM images of (a) the starting WO_3 powder, (b) the LPPS WO_3 coating, (c) the SPS WO_3 coating deposited using the spray power of 30 kW, and (d) the SPS WO_3 coating deposited using the spray power of 33 kW. The insets in (b, c, d) are enlarged views of typically selected areas. (e, f) High resolution TEM images of the SPS coating.

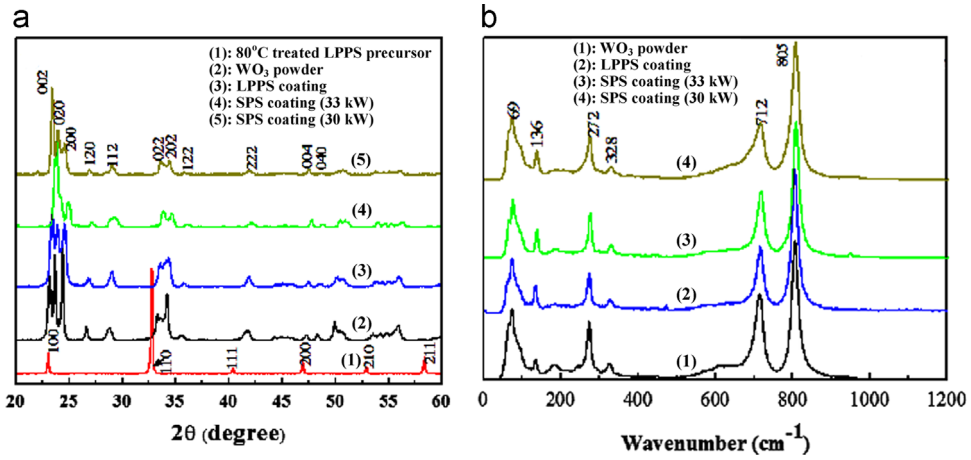

Fig. 2. XRD patterns (a) and Raman spectra (b) of the samples.

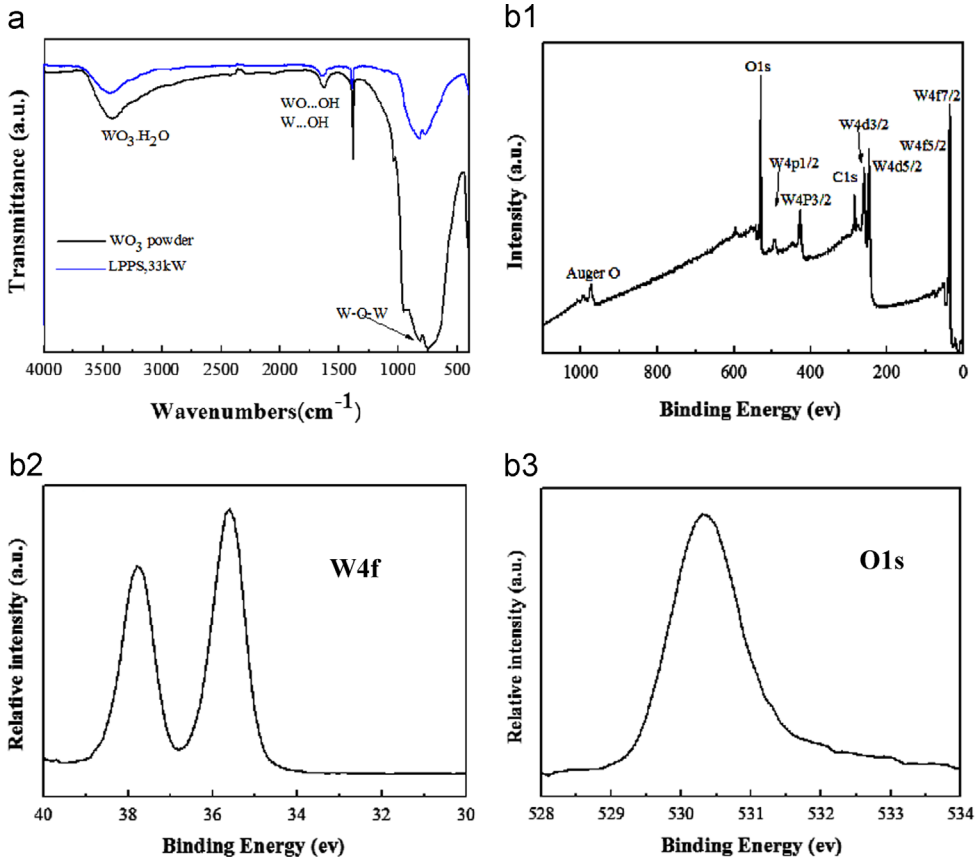

Fig. 3. FTIR spectra (a) and XPS survey scan (b-1) of the LPPS coating, the XPS curves for W4f (b-2) and O1s (b-3) are shown separately.

phonon bands at 805 cm^{-1} and 712 cm^{-1} are assigned to the O-W-O stretching mode and the peak at 805 cm^{-1} refers to the vibration of shorter bonds. The W-O-W bending mode of bridging oxygen is located at 272 cm^{-1} and 328 cm^{-1}, and the peak located at 136 cm^{-1} is for lattice vibrations of WO_3 [16]. Those bands are typical ones for monoclinic WO_3. The starting WO_3 powder and the LPPS coating were also examined by FTIR and XPS (Fig. 3). W-OH and W-O-W are realized in both the powder and the coatings, which is evidenced by the appearance of the peaks located at ~1630 and ~838 cm^{-1}. However, it is noted that for the coating sample, the IR peaks for W-O-W and W…OH exhibit remarkable differences from those for the WO_3 powder. This might indicate certain changes in chemistry of the pyrolysis synthesized WO_3 compared with the commercial WO_3.

To further clarify the changes, surface chemical composition and electronic structure of the LPPS coating were determined by XPS detection (Fig. 3b). The XPS spectrum for the element W shows the usual $4f_{5/2}$ and $4f_{7/2}$ doublets at 37.8 and 35.6 eV respectively, which agree well with the literature value for W^{6+} [17]. There is therefore conclusive evidence that the valence state of W is solely +6 [18]. The binding energy peak of O_{1s} can be observed at 530.3 eV, which is very close to the characteristic Eb of O in WO_3, 530.6 eV [3]. These results infer that the stoichiometry of the tungsten oxide formed during the coating processing is WO_3.

Large surface area is essential for attaining favorable performances for gas-sensing coatings. The porous WO_3 coatings reported here are able to provide more gas adsorption sites for the reaction related to gas detection. The tunable nanostructures of well-crystallized WO_3 not only are promising for applications for gas sensing, but also open a new window for constructing desirable structures for other functional applications.

4. Conclusions

A simple approach was proposed to deposit porous nanostructured WO_3 coatings for gas-sensing applications. The nanostructural features are tunable as achieved by adjusting the spray power or deposition methods. The formation of planar WO_3 grains with oriented grain growth along the (0 0 2) plane was revealed. The nanostructured coatings exhibit great potential for gas-sensing and other functional applications.

Acknowledgments

This research was supported by National Natural Science Foundation of China (grant # 31271017 and 41476064), Ningbo International Collaboration Project (grant # 2012D10010) and 100 Talents Program of Chinese Academy of Sciences.

References

[1] Wetchakun K, Samerjai T, Tamaekong N, Liewhiran C, Siriwong C, Kruefu V, et al. Sensor Actuat B-Chem 2011;160:580–91.
[2] Zhang C, Van Overschelde O, Boudiba A, Snyders R, Olivier M-G, Debliquy M. Mater Chem Phys 2012;133:588–91.
[3] Cantalini C, Sun HT, Faccio M, Pelino M, Santucci S, Lozzi L, et al. Sensor Actuat B-Chem 1996;31:81–7.
[4] Patra A, Auddy K, Ganguli D, Livage J, Biswas PK. Mater Lett 2004;58:1059–63.
[5] Abe Y, Ishiyama N. Mater Lett 2007;61:566–9.
[6] Tamaki J, Hayashi A, Yamamoto Y, Matsuoka M. Sensor Actuat B-Chem 2003;95:111–5.
[7] Gao X, Yang C, Xiao F, Zhu Y, Wang J, Su X. Mater Lett 2012;84:151–3.
[8] Shankar N, Yu MF, Vanka SP, Glumac NG. Mater Lett 2006;60:771–4.
[9] Hemberg A, Konstantinidis S, Viville P, Renaux F, Dauchot JP, Llobet E, et al. Sensor Actuat B 2012;171-172:18–24.
[10] Zhang C, Debliquy M, Liao H. Appl Surf Sci 2010;256:5905–10.
[11] Guo W, Liu T, Zeng W, Liu D, Chen Y, Wang Z. Mater Lett 2011;65:3384–7.
[12] Guo C, Yin S, Yan M, Kobayashi M, Kakihana M, Sato T. Inorg Chem 2012;51:4763–71.
[13] Calavia R, Mozalev A, Vazquez R, Gracia I, Cane C, Ionescu R, et al. Sensor Actuat B-Chem 2010;149:352–61.
[14] Chraska T, King AH. Thin Solid Films 2001;397:30–9.
[15] Cantalini C, Pelino M, Sun HT, Faccio M, Santucci S, Lozzi L, et al. Sensor Actuat B 1996;35:112–8.
[16] Siciliano T, Tepore A, Micocci G, Serra A, Manno D, Filippo E. Sensor Actuat B-Chem 2008;133:321–6.
[17] Garavand NT, Mandavi SM, Irajizad A, Ahadi K. Mater Lett 2012;82:214–6.
[18] Fruhberger B, Grunze M, Dwyer DJ. Sensor Actuat B-Chem 1996;31:167–74.